JOURNAL OF MATERIALS SCIENCE **34** (1999) 307–322

Formation of titanium carbonitride phases via the reduction of TiO_2 with carbon in the presence of nitrogen

ANIMESH JHA
Department of Materials, University of Leeds, Clarendon Road, Leeds, LS2 9JT, UK
S. J. YOON
Department of Materials Science, Miryang University, Miryang, South Korea

The reduction of rutile (TiO_2) with carbon was studied in a range of nitrogen atmospheres. The effect of the reactivity of carbon on the reducibility of TiO_2 to titanium carbonitride phase (TiC_xN_y) was investigated over a range of temperatures between 1173 K and 1773 K. The present study also reports the effect of the presence of ammonia, CO, and hydrogen gases on the reduction reaction equilibrium of TiO_2 to carbonitride (TiCN). The compositional dependence of the lattice parameter of TiCN phase on the concentrations of interstitial atoms, C, N, and O is also discussed. The mechanism of TiCN phase formation from TiO_2 has been established on the basis of a predominance area diagram in the Ti–C–N–O system derived from the Gibbs free energy data at 1573 K and 1 atm of N_2 gas. The derived values of the activation energies for simultaneous reduction-nitridation of TiO_2 to TiCN are discussed in the light of interstitial ion diffusion through the B1 (NaCl type) structure. The dependence of TiC lattice parameter on the concentrations of N and O at the interstitial sublattice sites is also established. The apparent values of the activation energies were found to be in the range of 220 kJ to 240 kJ mol^{-1} for both types of reducing agents: graphite and activated charcoal.

1. Introduction

Titanium nitride ($Ti_{1+x}N_{1-x}$) is an interstitial compound with a large concentration of N atom vacancies ranging from 23 at % to 50 at % nitrogen [1]. The crystalline phase (B1–NaCl type) has an fcc structure and exhibits both covalent and metallic characteristics. The material, as a result, has high melting point (3223 K), thermal conductivity (1.92–2.09 $Jm^{-1}\,s^{-1}\,K^{-1}$), low resistivity (10^{-3}–10^{-4} Ω cm), isotropic expansion coefficient (9.3×10^{-6} K^{-1}), oxidation resistance up to 1200 K, high hardness, and fracture toughness (6–10 $MPam^{1/2}$) [2].

Over the last two decades, the main emphasis in designing engineering materials and components has been to achieve better performance in service conditions. The development of the modern cutting tool is a good example of a well-engineered material that is a multilayered structure of ceramics on a tungsten carbide substrate [3]. TiN is an important ingredient of the layered structure that contributes to the improvement in the oxidation resistance, fracture toughness, and heat conduction. TiC and TiN provide a better adhesion with the metallic substrate [4]. $Ti_{1+x}N_{1-x}$ and TiCN are used for strengthening ferrous matrices for wear-resistant surfaces [5, 6]. The main advantage of using TiN or TiCN is that it not only has a better adhesion with the ferrous alloy matrix, but also improves the oxidation resistance, which is not possible when tungsten carbide is used as a wear-resistant material for surfaces at elevated temperatures. Carbides, nitrides, and borides of titanium are potential candidates for reinforcing copper power transmission cables [7]. The hardness and stiffness of TiN and TiB_2, which is higher than that of the copper cable, enhances the stiffness, which could lead to a major reduction in the installation of number of pylons required for supporting the power transmission cables. Another important contribution of TiN in the Cu-alloy matrix is to reduce the penalty on power transmission loss [7]. The high thermal conductivity and oxidation resistance makes this material an important constituent for designing a new generation of advanced ceramic refractory materials for continuous casting of steel.

In the close-packed face-centered cubic lattice (B1, NaCl type), N atoms partly occupy interstitial sites, leaving remaining sites vacant; as a result, the N-deficient sites in the structure range from 0 to 27 at % N in the $Ti_{1+x}N_{1-x}$ structure. Above a Ti:N ratio equal to unity, the Ti-deficient sites appear. Consequently, the lattice parameter of the TiN phase, which increases between 23 at % N and 50 at % N, falls rapidly above a Ti:N ratio less than unity [1, 2, 8]. The concentration of N also determines the physical properties of the ceramic phase. For example, when the Ti:N ratio is more than 1, the ceramic exhibits more metallic characteristics,

which diminishes with increasing N occupancy in the lattice. The N-rich phases are more covalent than is the composition, with the Ti:N ratio greater than the unity. Some of the important applications of TiN and TiC are for making multilayer-coated structures for the tips of cutting tools, electromachinable ceramics, and metal evaporator boats and for thermal barrier coatings [9].

In this paper, we examine the role of the processing conditions on the chemical composition and lattice parameter of TiN structure during the carbothermic reduction of TiO_2 in the presence of a range of N atmosphere. We also report the thermodynamic phase equilibria in the Ti–C–N–O system. The rate of reduction of TiO_2 is examined, and the results of the temperature coefficient of overall rate of reduction with graphite and charcoal are also compared.

2. Literature

Polycrystalline $Ti_{1+x}N_{1-x}$ are usually prepared via the powder metallurgical route during which Ti metal powder is nitrided using N or ammonia (NH_3) gas [10]. Titanium hydride is also used in the place of metallic Ti [11–13]. The nitriding of metal or metal hydride is an exothermic reaction: $Ti\,(s) + 1/2\,(N_2)_{gas} = TiN$ or $TiH\,(s) + 1/2\,(N_2)_{gas} = TiN + 1/2\,(H_2)_{gas}$. The chemical vapour deposition (CVD) route involves reaction between titanium tetrachloride ($TiCl_4$) and NH_3 [14] in the gaseous phase via $TiCl_4\ (g) + 4/3\,(NH_3)_{gas} = TiN + 4(HCl)_{gas} + 1/6\,(N_2)_{gas}$. Alternatively, the oxides are reduced in the presence of N to form metal nitride. Mixed interstitials, for example TiCN and titanium oxycarbonitride (TiOCN), can also be synthesized via this route [15–20]: $TiO_2 + 1/2\,N_2 + 2C = TiN + 2CO$. The major advantage of the carbothermic reduction compared with CVD and metal powder nitridation processes is that it relies on the supply of inexpensive raw materials, and the process is capable of yielding TiCN with a range of N and C content. This technique, therefore, can be adopted in designing a functionally gradient ceramic material, in which the physical properties of the material can be tailored between TiC and TiN by setting C and N potentials for achieving a concentration gradient of C and N, respectively. Li and Riley [17], Licko *et al.*, [18] and White and co-workers [19, 20] have studied the reduction and nitridation of TiO_2 and anatase for making TiN and TiCN phases. The overall activation energy for the nitridation of TiO_2 in the temperature range of 1473 to 1693 K was found be 260 kJ mol^{-1}. The reaction sequence identified by previous investigators [17–20] was $TiO_2 \rightarrow Ti_nO_{2n-1} \rightarrow Ti_3O_5 \rightarrow TiN_{1-x-y}O_yC_x$. No evidence for the existence of either Ti_2O_3 or TiO was found to support the mechanism described by Umezu [16]. White *et al.* [19] pursued the hypothesis proposed by Lyubimov *et al.* [15] that in the absence of CO_2 in the outlet gas, not being detected by mass spectrometry, C_3O_2 ought to be an important intermediate gaseous species for sustaining the overall reduction. White *et al.* [19, 20], however, overlooked the Boudouard reaction: $2CO\,(g) \rightarrow C + CO_2\,(g)$, which is known to be responsible for carbon deposition in the stack region of iron blast furnaces [21] and in the reduction kiln [22]. C_3O_2 is unstable at 1 atm condition of CO gas, whereas both C deposition and C dissolution can occur via the Boudouard reaction at 1 atm, [23] at which most of the TiCN formation reaction has been studied, including those studies of White *et al.* [19, 20]. In the present work, experimental data for activation energies are compared with the data from the literature [15–20].

3. Experiments

Pigment-grade TiO_2 that had a surface area of 40–50 $m^2\ g^{-1}$ and C in the graphitic and charcoal forms were used as the starting materials. The average particle size of TiO_2 was below 500 nm, whereas the average size of the graphite and charcoal flakes was approximately 15–30 μm. TiO_2 and carbon were weighed in stoichiometric amounts. The weighed materials were dry mixed thoroughly, ground in an agate mortar and then pressed in a 6-mm inner diameter steel die to form cylindrical pellets. The pressure used was 30 MPa. A silicon carbide resistance tube furnace was employed for heating the pelletized mixtures. Prior to isothermally heating the pellets, these samples were transferred inside a graphite crucible. The pellets were held for several hours by selecting an isotherm in the range of 1173 to 1823 K. Each pellet took less than 3 min to reach the selected isotherm. It was recorded that the weight loss sustained by a pellet while reaching an isotherm was insignificantly small in comparison with the total expected weight loss. The N_2 gas was dried using silica gel and anhydrous sodium carbonate. Prior to heating the sample in the reaction chamber, it was purged with N_2 gas for several minutes in order to remove the residual O_2. The gas flow rate in all experiments was 500 mL min^{-1}.

After each isothermal hold, the pellets were weighed for the calculation of percentage reduction using the formula $\%R = (W_t/W_o) \times 100$, where W_t is the total weight loss sustained by the pellet at a given time t and W_o is the total stoichiometric weight loss determined from the reaction, for example: $TiO_2 + 2C + 1/2\,N_2 = TiN + 2CO\,(g)$. In some reactions, an excess of carbon (TiO_2:C > 2–3) was added for studying the effect of the enhanced reduction reaction surface area. For these reactions with excess carbon, the values of W_o were recalculated for obtaining the corresponding values of %R as a function of time. The phases present in the reacted pellets were determined by X-ray powder diffraction technique using Cu-kα radiation at 0.15406 nm wavelength. The powder diffraction results were used for determining the lattice parameters of the TiN phase for a given set of processing conditions.

A limited number of experiments were also carried out with the addition of ferric chloride ($FeCl_3 \cdot 6H_2O$) as a catalyst for ascertaining the changes in the overall rate of reaction with graphite as a reducing agent.

4. Results

4.1. Analysis of the phases formed

The reduced pellets were examined by X-ray powder diffraction technique for the identification of phases.

TABLE I The Gibbs free energy functions and the equilibrium CO gas partial pressures in the TiO_2-C-N_2 system, indicating the stability ranges for various suboxides. Gibbs free energy equations were derived from the data in [29]

Reaction	ΔG°_T, J mol^{-1}	T_{eq}, K	P_{CO}, atm
$3TiO_2 + C = Ti_3O_5 + CO$	273 595 - 198.1 T	1381	18.3
$2Ti_3O_5 + C = 3Ti_2O_3 + CO$	249 740 - 152.8 T	1634	0.48
$Ti_2O_3 + C = 2TiO + CO$	358 575 - 195.9 T	1830	0.021
$TiO_2 + 2C + 1/2\,N_2 = TiN + 2CO$	376 070 - 256.0 T	1469	7.65
$TiO_2 + 3C = TiC + 2CO$	527 685 - 336.7 T	1567	1.16

Crystalline phases such as $Ti(C_xN_{1-x})$, TiO_2, Ti_xO_y, Ti_3O_5, and C were identified. TiO_2, under reducing conditions, can produce a series of non-stoichiometric phases such as Ti_3O_5, Ti_4O_7, and Ti_7O_{13}, but in this experiments only Ti_3O_5 and non-stoichiometric Ti_xO_y $(x/y > 3/5)$ phases were identified. Ti_2O_3 was not identified in the reaction product and was found to be in disagreement with the experimental findings of Terry and Chinyamakaobru [6]. The thermodynamic reason for the absence of Ti_2O_3 during the reduction nitridation of TiO_2 is discussed later. The removal of oxygen from the TiO_2 lattice occurs during reduction leading to the formation of a non-stoichiometric Ti_xO_y phases, and Ti_3O_5 is one such example of an intermediate phase. The above observations are consistent with those made by Li and Riley [17], Licko *et al.* [18], and White *et al.* [19, 20]. Among the non-stoichiometric phases, the order of emergence of suboxide phases was Ti_5O_9, Ti_4O_7, and Ti_3O_5, the higher suboxides being more stable at lower temperatures than Ti_3O_5 was. The observation of higher suboxides in partially reduced samples was also found to be consistent with the stability of the suboxides in the Ti–O phase diagram [24], reported elsewhere. The non-stoichiometric Ti_3O_5 phase therefore appears to be an important reaction intermediate at higher temperatures for sustaining the nitridation reaction, which is finally reduction nitrided to a TiCN phase with a release of CO gas via: $Ti_3O_5\,(s) + (5 + 3x)C\,(s) + 3y/2N_2\,(g) = 3\,TiC_xN_y + 5\,CO\,(g)$. Ti_3O_5 also formed when 50 vol % N_2, 25 vol % H_2, 25 vol % CO gas mixture (designated here after $N_2 + H_2 + CO$ gas) was used as a purging and reducing gas in the reaction chamber. The reduction of TiO_2 could be a multistage reaction during which various suboxides and C establish equilibrium with CO gas, as described in Table I. In Table I, T_{eq} is the equilibrium temperature at which $\Delta G^o = 0$. Various suboxide phases formed over a range of temperatures with graphite and activated charcoal are compared in Table II, which points out that the activated charcoal is a more effective reducing agent than C. This is because the formation of TiN was confirmed comparatively at a much shorter period of time with activated charcoal than observed in the case of graphite. A comparison of X-ray powder diffraction patterns of phases formed is shown in Fig. 1. The suboxide phases formed during the reduction and nitridation of TiO_2 with activated charcoal, for example, in N_2 atmosphere are shown in Fig. 1. TiO_2 has a tetragonal structure, whereas the suboxides with O:Ti ratio greater than 1.75 have a triclinic structure. The lower suboxides, namely, Ti_3O_5, Ti_2O_3, α-TiO, and β-TiO have monoclinic, trigonal, monoclinic, and cubic structures, respectively, as

TABLE II Summary of phases formed after stages I, II, and III. Phases are arranged in the decreasing order of relative intensities. Mixture composition: TiO_2:C = 1:3

T, K	Time, h	Phases identified	
		Graphite reductant	Charcoal reductant
1473	0.1	regime I: C, Ti_9O_{17}, TiO_2^{**}	Ti_5O_9, Ti_4O_7: regime I
	0.2	regime I: C, Ti_9O_{17}, Ti_8O_{15}	Ti_4O_7, Ti_5O_9: regime II
	0.3	regime I: C, Ti_6O_{11}, Ti_7O_{13}, Ti_8O_{15}	Ti_4O_7, Ti_3O_5: regime II
	0.7	regime II: C, Ti_6O_{11}, Ti_5O_9, $Ti_7O_{13}^{**}$	Ti_3O_5, TiCN: regime II
	4.0	regime III: C, Ti_3O_5, TiCN**	Ti_3O_5, TiCN: regime III
	8.0	regime III: C, Ti_3O_5, TiCN**	TiCN, Ti_3O_5: regime III
1573	0.1	regime I: C, Ti_4O_7, Ti_3O_5	Ti_3O_5, TiCN: regime I
	0.2	regime I: C, Ti_3O_5, Ti_4O_7	Ti_3O_5, TiCN: regime II
	0.7	regime II: C, Ti_3O_5, TiCN	TiCN, Ti_3O_5: regime II
	4.0	regime III: C, Ti_3O_5, TiCN	TiCN: regime III
	8.0	regime III: C, Ti_3O_5, TiCN	TiCN: regime III
1673	0.1	regime I: C, Ti_3O_5, TiCN	TiCN, Ti_3O_5: regime I
	0.2	regime I: C, Ti_3O_5, TiCN	TiCN, Ti_3O_5: regime I
	0.7	regime II: C, Ti_3O_5, TiCN	TiCN: regime II
	4.0	regime III: C, TiCN, Ti_3O_5	TiCN: regime III
	8.0	regime III: C, TiCN, Ti_3O_5	TiCN: regime III
1773	0.1	regime I: C, Ti_3O_5, TiCN	TiCN: regime I
	0.7	regime II: C, TiCN, Ti_3O_5	TiCN: regime II
	4.0	regime III: TiCN, C	TiCN: regime III
	8.0	regime III: TiCN, C	TiCN: regime III

**designates a trace amount of the phase.

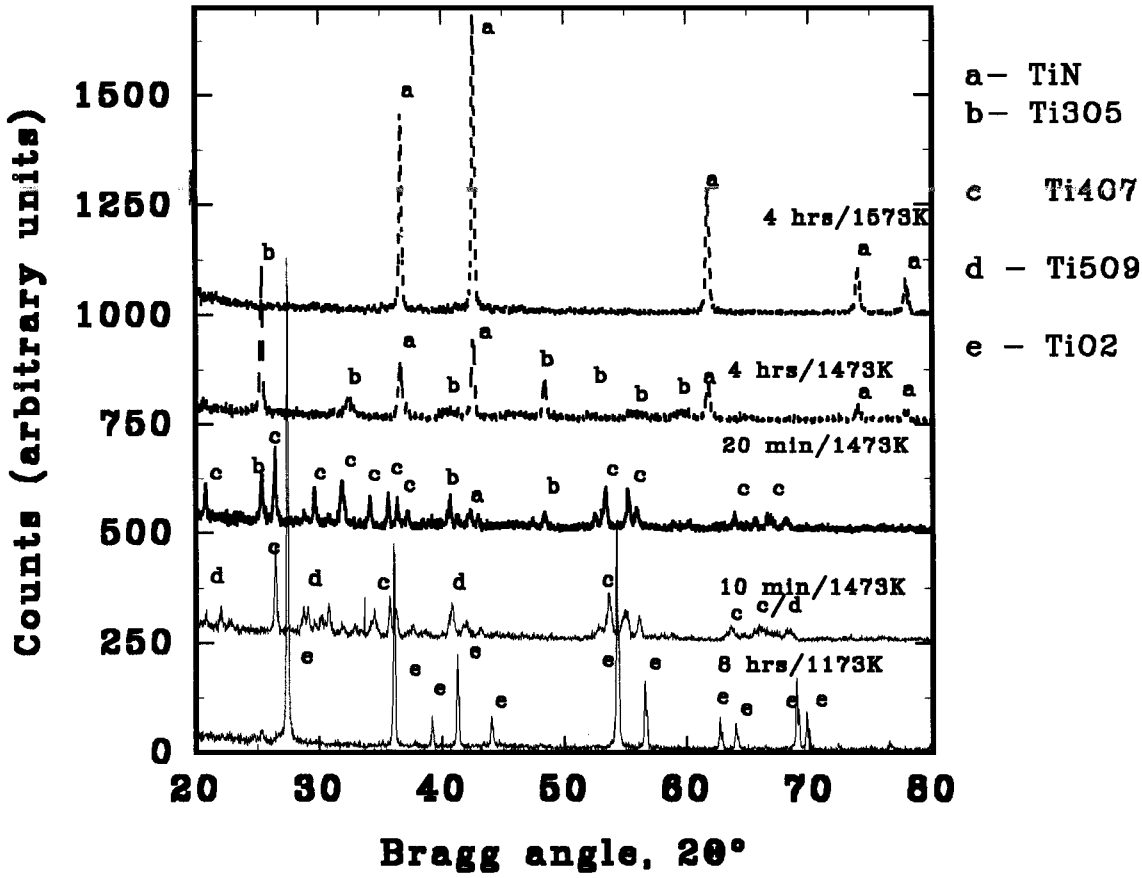

Figure 1 A comparison of X-ray powder diffraction patterns for TiO_2:C = 1:3 (activated charcoal) over a range of temperatures and time periods indicated in the figure.

can be seen in Table III. From the equilibrium conditions at 1573 K shown in Table I, for example, for the reduction and subsequent nitridation of suboxides to TiN, it is evident that the values of the equilibrium partial pressures of CO for the stability of Ti_3O_5 and TiN are much larger than those for Ti_2O_3 and TiO. The values of P_{CO} must be less than 0.5 and 0.021 atm, respectively, at 1573 K for the stability of these two oxides.

4.2. The effect of a carbonaceous atmosphere

The effect of the presence of gaseous mixtures of CO, H_2, and N_2 on the phases formed during the reduction of TiO_2 with C is shown in Table IV. The reduction and nitridation of TiO_2 to carbonitride phases, as shown in Table I, is dependent on the equilibrium partial pressure of CO gas in the ambient. This means that as the partial pressure of CO in the incoming gas increases, the equilibrium for each reaction described in Table I shifts to the left. This is because for the mixture containing TiO_2:C = 1:3 stoichiometric ratio, the amount of unreacted Ti_3O_5 is less in the N_2 atmosphere compared with the same mixture when reacted in an atmosphere of $(N_2):(CO + H_2) = 1:1$ by volume. The percentage reduction (%R) recorded for the $(N_2 + CO + H_2)$ gas mixture is 47.4 compared with more than 53.8 %R for graphite as a reducing agent in a N_2 gas at 1673 K (see Tables II and IV).

When the graphitic C was replaced by activated charcoal for $(N_2):(CO + H_2) = 1:1$ gas mixture, the percentage reduction observed was over 100. This is due to the loss of C from the starting mixture in the form of methane gas via C in the presence of a H reaction: $C + 2H_2\,(g) = CH_4\,(g)$. The resultant phase, however, was TiCN and no oxide was found to be present in the

TABLE III The crystal structure and lattice parameters of titanium oxides from JCPDS data file

Oxides	Crystal structure	Lattice parameters						JCPDS card ref. N°
		a, nm	b, nm	c, Å	α°	β°	γ°	
TiO_2	tetragonal	0.4593	0.4593	0.2959	90	90	90	21-1276
Ti_9O_{17}	triclinic	0.557	0.71	2.215	97.1	131.0	109.8	18-1405
Ti_4O_7	triclinic	0.560	0.713	1.246	95.1	95.1	108.8	18-1402
Ti_3O_5	monoclinic	0.9828	0.3776	0.9898	90.0	91.3	90	23-606
Ti_2O_3	trigonal	0.5139		1.366				10-63
TiO-Ó	monoclinic	0.585	0.934	0.414	90	90	107.5	23-1078
TiO-β	cubic	0.420	—	—	90	90	90	—

TABLE IV Phases formed after 4 h of the reduction of TiO_2 and C mixtures in the presence of carbonanceous gas ($CO + H_2$) mixtures. Phases are arranged in the descending order of the relative intensity

Starting materials TiO_2:C =	T, K	%R at 4 h	Gas mixture, vol % N_2	CO	H_2	Phase formed
		56.0	100	—	—	Ti_3O_5, C, TiCN
1:1	1673	45.3	65	17.5	17.5	Ti_3O_5, C,TiCN
		32.7	55	22.5	22.5	C, Ti_3O_5, TiCN
1:1 (AC)	1673	63.8	100	—	—	Ti_3O_5, TiO_2, TiCN
1:1 + $FeCl_3$	1673	75.8	50	25	25	TiCN, Ti_3O_5
1:2	1673	30.6	55	22.5	22.5	C, Ti_3O_5, TiCN
		53.8	100	—	—	C, TiCN, Ti_3O_5
1:3	1673	71.3	75	—	25	TiCN, C, Ti_3O_5
		47.4	50	25	25	C, Ti_3O_5, TiCN
		109.4	100	—	—	TiCN
1:3 (AC)	1673	119.2	75	25	—	TiCN
		112.4	50	25	25	TiCN

Starting mixtures, TiO_2:C=	T, K	t, h	%R	Gas mixture, vol % Ar	NH_3	H_2	
1:2	1673	2	88.3	100	—	—	TiCN, Ti_3O_5
	1473	2	48.7	62.4	35	2.6	TiCN, Ti_3O_5
	1573	2	51.8	62.4	35	2.6	TiCN, Ti_3O_5
		4	74.6	72	25	3	TiCN, Ti_3O_5
	1673	2	61.2	62.4	35	2.6	TiCN, Ti_3O_5
		4	100.9	62.4	35	2.6	TiCN
1:1	1473	2	68.3	62.4	35	2.6	TiCN, Ti_3O_5
	1573	2	75.4	62.4	35	2.6	TiCN, Ti_3O_5
	1673	2	76.2	62.4	35	2.6	TiCN, Ti_3O_5

reaction product. Graphite in the presence of $CO + H_2$ gas (Table IV) was found to be a less effective reducing agent compared with charcoal, and it is for this reason that the observed percentage reduction was much higher for activated charcoal than it was in graphite. A mixture containing TiO_2 with 1 mol of C (TiO_2:C = 1:1) was reduced in ($CO + H_2$) atmosphere mixed with N_2 at 1673 K for different lengths of time. The time dependence of the percentage reduction for TiO_2:C = 1:1 stoichiometric mixture is also shown in Table IV.

4.3. Effect of ammonia gas atmospheres and $FeCl_3 \cdot 6H_2O$ as a catalyst

Mixtures of TiO_2 and C were reduced in a gaseous mixture of 96 vol % Ar, 4 vol % H_2, and NH_3. This gas mixture will be designated from here on as ($Ar + NH_3 + H_2$) gas mixture. The concentrations of ammonia gas in volume percent are indicated in Table IV. With increasing concentration of NH_3 in the gaseous phase, the value of percentage reduction was found to increase at a given temperature. The percentage reduction also increased with increasing time and temperature. The values of percentage reduction in Table IV for nitridation of TiO_2 plus C mixtures with the $NH_3 + H_2 + Ar$ gas mixture can be compared with the data for $CO + H_2 + N_2$ mixture shown in the same table.

A limited number of experiments were carried with $FeCl_3 \cdot 6H_2O$ as a catalyst. Graphite powder was mixed with 5 wt % $FeCl_3 \cdot 6H_2O$, and the results are compared with catalyst at 1673 K in Fig. 2. While plotting these results, the weight loss due to the liberation of H_2O and Cl_2 was also accounted for, calculating the values of percentage reduction. The results, shown in Table V and Fig. 2 confirm that the presence of a catalyst greatly increases the rate of reaction.

4.4. Comparison of the rates of reactions with graphite and activated charcoal as reducing agents

The rates of reduction of TiO_2 to TiCN at different isotherms for graphite and activated charcoal are compared in Figs 3 and 4, respectively, from which it is evident that the type of carbon, in this case active charcoal, has a pronounced effect in determining the speed of the chemical reaction. When graphite was used as a reducing agent (Fig. 3), for example, the reduction reaction stagnated at about 20 %R after 1 h reaction at 1473 K. For activated charcoal as a reducing agent, nearly 60 %R, as can be seen in Fig. 4, was achieved after 1 h at 1473 K. The reaction reached completion after 4 h at 1573 K. Activated charcoal is known to have a large surface area and reactivity compared with

TABLE V The effect of ferric chloride catalyst on the reducibility of TiO_2 to TiN phases at 1673 K. (TiO_2:C = 1:3) in N_2 atmosphere

Time, h	TiO_2:3C at 1673 K	TiO_2:3C with 5% $FeCl_3$ at 1673 K
0.0	0.0	0.0
0.2	24.6	34.6
1.0	34.7	64.0
4.0	53.8	95.9
8.0	70.1	103.5

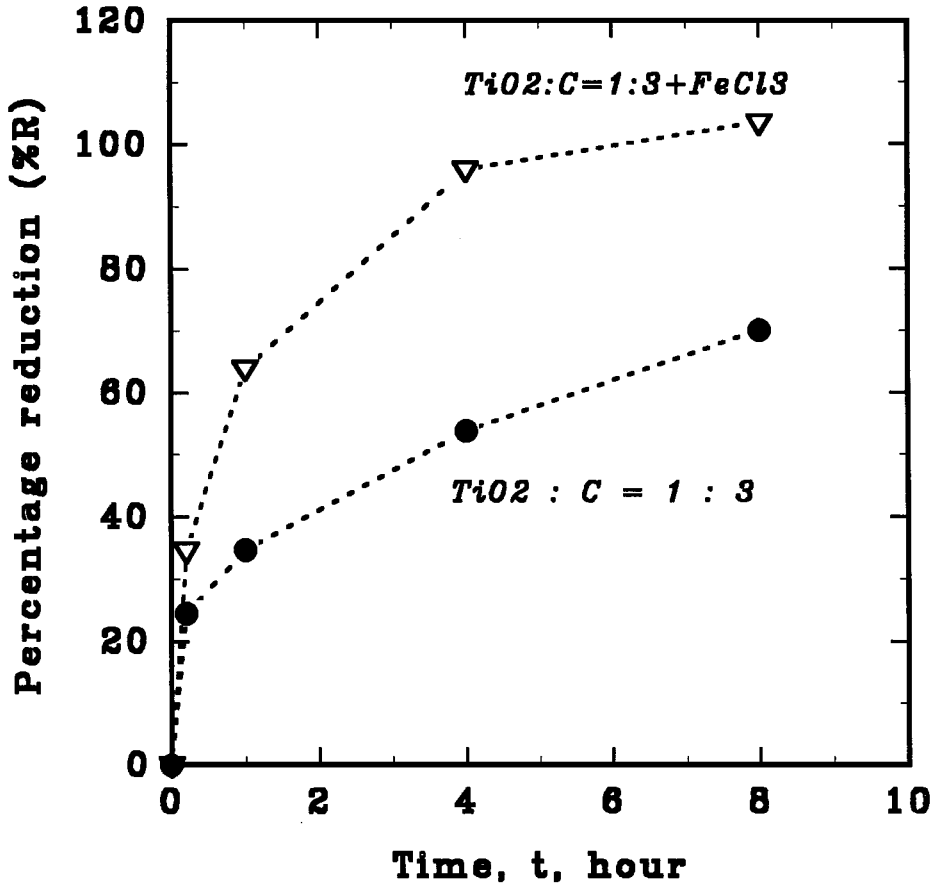

Figure 2 Comparison of the rates of the reduction-nitridation of TiO_2 with carbon (TiO_2:C = 1:3) in the presence of hydrated ferric chloride as a catalyst.

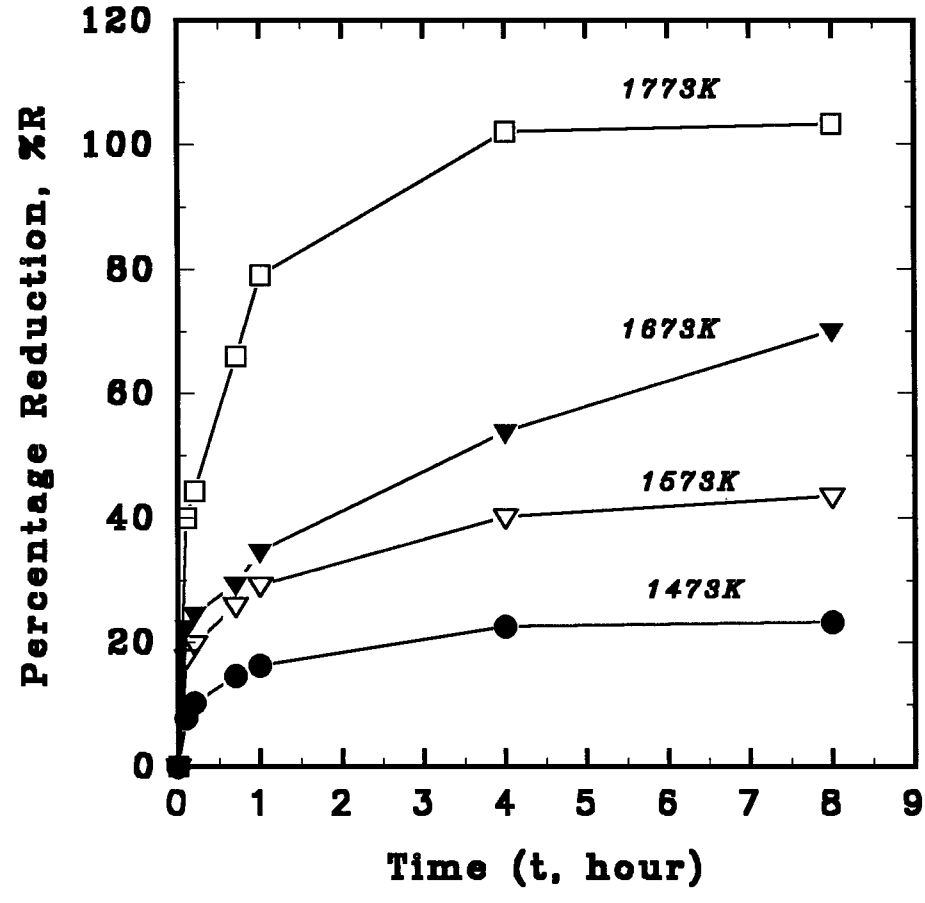

Figure 3 Rates of simultaneous reduction-nitridation of TiO_2 with graphite in N_2 atmosphere at various temperatures.

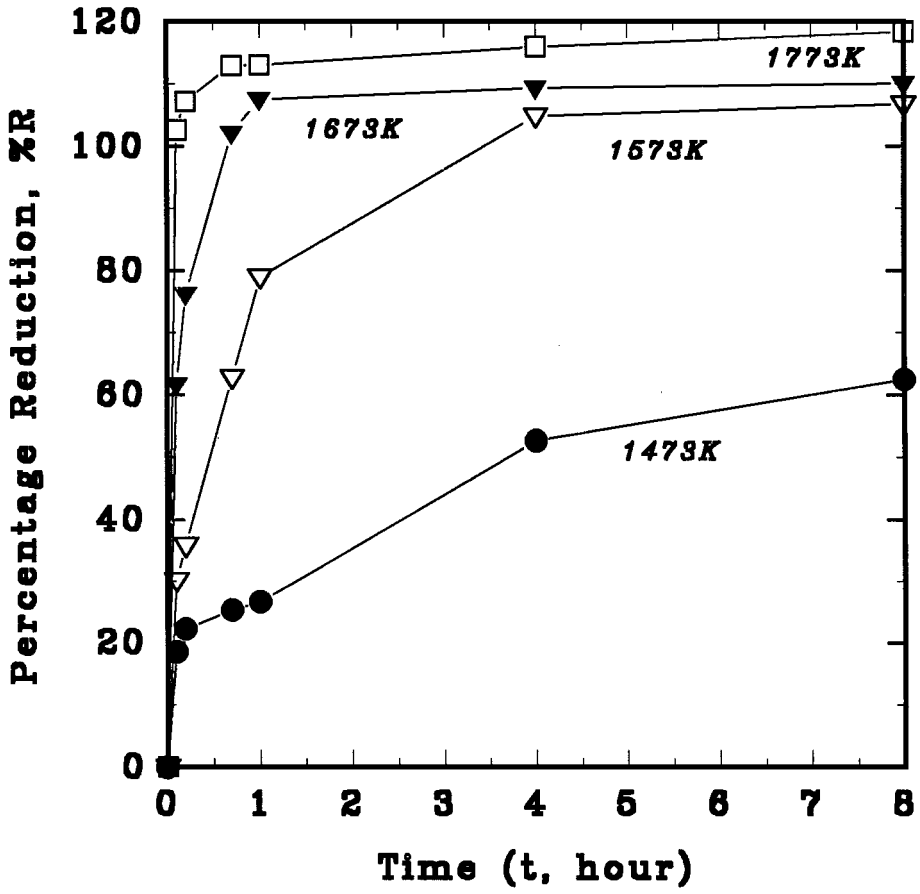

Figure 4 Rates of simultaneous reduction nitridation of TiO_2 with activated charcoal in N atmosphere at various temperatures.

graphite. It also provides an increased number of active sites for the adsorption of oxygen, an essential requirement for the nucleation of CO, the mechanism for which is illustrated elsewhere [25, 26]. The values of percentage reduction for various time durations at each temperature for graphite and activated charcoal are compared in Table VI. With the increasing reduction temperature, the conversion of TiO_2 to a carbonitride phase occurred readily. TiCN was the main product of the reaction. For intervals longer than 40 min, Ti_3O_5 had completely converted to TiCN at 1673 K. By lowering the isotherm by 100 K to 1573 K, however, a much longer completion time resulted, in this case 8 h. Significant nitridation was observed above 22 %R, and Ti_3O_5 was found to exist from about 18 to 80 %R along with TiCN. This is exemplified by the reduction data in Table VI, when TiO_2 was reduced in an atmosphere of CO (25 vol %), H_2 (25 vol %), and N_2 (50 vol %) gas mixture. Above the stoichiometric molar ratio of C:$TiO_2 = 2$, the rate of formation of TiCN was found to be appreciable and depended strongly on the reactivity of C, for example, the active C accelerated the TiO_2 to TiCN conversion process. When active C was used as a reducing agent, 80% nitride phase was produced in less than 5 min of reaction time by carbothermic reduction above 1673 K, which is evident from Fig. 4. It was also observed that

TABLE VI The effect of activated charcoal and graphitic C on the values of percentage reduction as functions of time and temperature

Time (t), h	%R at 1473 K	%R at 1573 K	%R at 1673 K	%R at 1773 K
	Reduction of TiO_2:C = 1:3 in N_2 atmosphere. Carbon used was graphite			
0.1	7.8	17.6	22.4	40.0
0.2	10.3	19.9	24.6	44.3
0.7	14.6	26.0	29.4	66.0
1.0	16.3	29.3	34.7	79.1
4.0	22.5	40.2	53.8	101.9
8.0	23.3	43.5	10.1	103.2
	Reduction of TiO_2:C = 1:3 in N_2 atmosphere. Carbon used was activated charcoal			
0.1	18.5	30.2	61.7	102.6
0.2	22.2	35.8	76.2	107.2
0.7	25.3	62.8	102.1	113.0
1.0	26.7	79.0	107.6	113.1
4.0	52.7	104.9	109.4	116.0
8.0	62.5	106.8	110.1	118.4

the total percentage reduction with the activated charcoal exceeded more than 100 %R. The total weight loss (or percentage reduction) with activated charcoal exceeded was well above 100 %R to 118 %R, approximately. This was due to the presence of residual levels of moisture (H_2O), which is slightly larger in molar mass than 1/2 mol of N_2 gas, and also due to the carbonitriding reaction: $TiN + C \rightarrow TiC + 1/2\,N_2$. The values of larger weight loss, therefore, designate a proportionately larger amount of C atoms replacing N atoms in the TiN crystal structure at interstitial sites.

4.5. Effect of time, temperature, and carbon content on the lattice parameter of TiN

The lattice parameter of the synthesized carbonitride phase was calculated from the measured d-spacing data derived from the X-ray powder diffraction peaks. TiN has a face centered cubic structure. The Bragg angle peaks corresponding to (1 1 1), (2 0 0), (2 2 0), (3 1 1), and (2 2 2) set of planes were used for determining the a-values. The data were statistically fitted to find a precise value of "a" by extrapolating the $\sin^2\theta$ linear function to a value of θ equals to 90°. The derived value of lattice parameter from each experiment was compared with the values of the stoichiometric TiN and TiC phases, and these are plotted against the atomic percent of interstitial atom composition in Fig. 5. Each lattice parameter plotted corresponds to a unique composition of C and N in the crystalline lattice of TiCN. The composition of C or N was calculated from Equation 2, which is the solution for Equation 1. In this equation, a^{TiC} and a^{TiN} are the lattice parameters of stoichiometric TiC and TiN, respectively. Multiplying X_c by 100 will yield atomic percentage of C.

$$a_{TiCN} = X_c \cdot (a^{TiC}) + (1 - X_c) \cdot (a^{TiN}) \quad (1)$$

$$X_c = \frac{(a^{TiCN}) - (a^{TiC})}{(a^{TiN}) - (a^{TiC})} \quad (2)$$

Note that the method adopted cannot yield the value of the total vacancy concentration in the TiCN lattice. In order to include the vacancy concentrations in the calculation, the lattice parameter of the non-stoichiometric TiC and TiN phases must be included. An identical metal to interstitial ratio per formula unit would mean that the total number of vacancies in each TiC and TiN lattice is fixed and is assumed to be randomly distributed. For example, Fig. 5 can also be drawn by considering the substoichiometric compositions (e.g., Ti:N = Ti:C = 1.1). It is evident from this figure that the nitrides of Ti formed as a result of the carbothermic reduction are the carbonitrides $Ti(C_xN_{1-x})$ and not the stoichiometric TiN phase. The non-stoichiometric range for $Ti_{1-x}N_x$ compounds extends from 23 to 57 at % N. During the reaction, C dissolves in the lattice by occupying the vacant interstitial sites and produces a TiC_xN_{1-x} phase. The dissolution of C atoms in the $Ti_{1-x}N_x$ lattice commences because of the comparable atomic radii of the two interstitial atoms, C and N. Licko *et al.* [18] chemically analysed the carbonitride phase and concluded that O atoms also

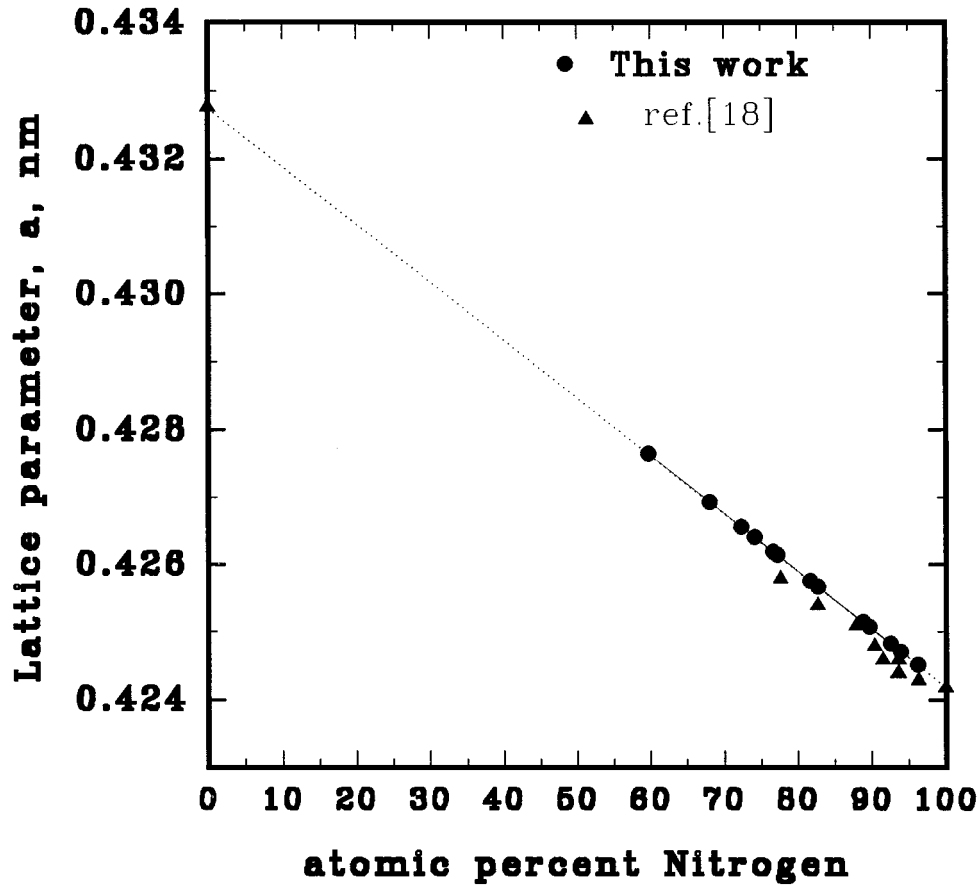

Figure 5 A plot of the lattice parameters of TiC and TiN and a comparison of the measured lattice parameters of interstitial solid solution phases with TiC and TiN cell dimensions.

occupy interstitial sites. Cubic $Ti_{1-x}O_x$, $Ti_{1-x}N_x$, and $Ti_{1-x}C_x$ have B1 NaCl structure; as a result, a mutual exchange of atoms at the interstitial sites in the crystal structure takes place. Grieveson [8] reported that the two interstitial compounds of Ti, in other words, TiN and TiC, do not mix ideally but exhibit a small negative departure from the ideal Raoultian behaviour. The departure from the ideal appears to become more apparent when more O atoms occupy the interstitial sites. The lattice parameters of TiCNO phases, determined by Licko *et al.* [18], hints that the oxygen-rich lattices may not follow the ideal solution behaviour.

We observed that when the H_2 gas was mixed with the bulk N during the reduction reaction, the tendency to form a carbonitride phase was significantly reduced. The N concentration then fell below 50 at %, in other words, to the right of the TiN (100%) composition.

The dependence of the lattice parameters on the time of reduction is plotted in Figs 6 and 7 for graphite and activated charcoal, respectively. From Figs 6 and 7, it is evident that the lattice parameters of the TiCN phase rise sharply in the initial phase of reaction and then drop before beginning to increase again at longer periods of time at each temperature. From Figs 6 and 7 and the observed changes in percentage reduction in Figs 3 and 4, it is apparent that the overall reaction can be divided into three different reaction stages: the *regime I* is the fastest, *regime II* follows after the initial fast stage, and the overall reaction terminates in *regime III*, which is the slowest step.

4.6. Microstructure

The scanning electron microscopic (SEM) examination revealed that the morphology of TiCN particles was strongly dependent on the reactivity of C, the gas mixture used, and the temperature. The grain morphologies of $Ti(C_xN_{1-x})$, shown in Figs 8 and 9, are the result of the difference in the reactivity of C. Fig. 9 also shows the morphology of unreacted activated charcoal platelets (pointed out as arrows), which suggests that the latter has approximately 10 μm average size flakes. The reduction of TiO_2 with activated C yielded finer grain size of the carbonitride phase at all temperatures compared with graphite as a reducing agent. In this case, the extent of sintering was also found to be small between the particles compared with the product derived from graphite as a reducing agent. In Fig. 10, the evidence for the difference in sintering of TiO_2 starting powder and the particulates of TiCN is presented, and these results are compared with the structure of the carbonitride phase in Fig. 9. It is evident that the flakes of graphite (shown as platelets) are bonded with the surrounding TiO_2 or suboxide particles. The reaction product after long reduction periods (>8 h) begins to sinter and facet. The sintering of TiCN particles does not appear to take place in a shorter period of time and at temperatures lower than 1673 K in the presence of activated charcoal as a reducing agent. These observations are consistent with the microstructural features reported by Li and Riley [17] and Licko *et al.* [18].

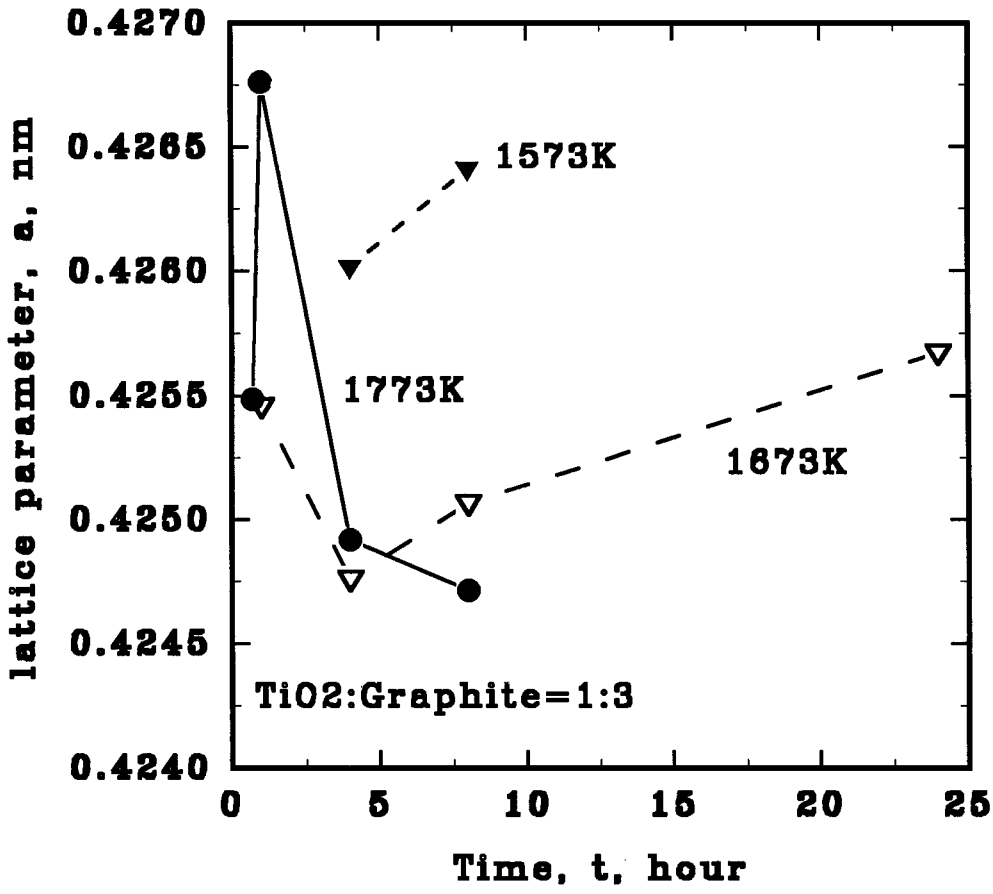

Figure 6 Effect of time and temperature on the lattice parameters of the carbonitride phase during the reduction nitridation of TiO_2 with graphite (TiO_2:C = 1:3).

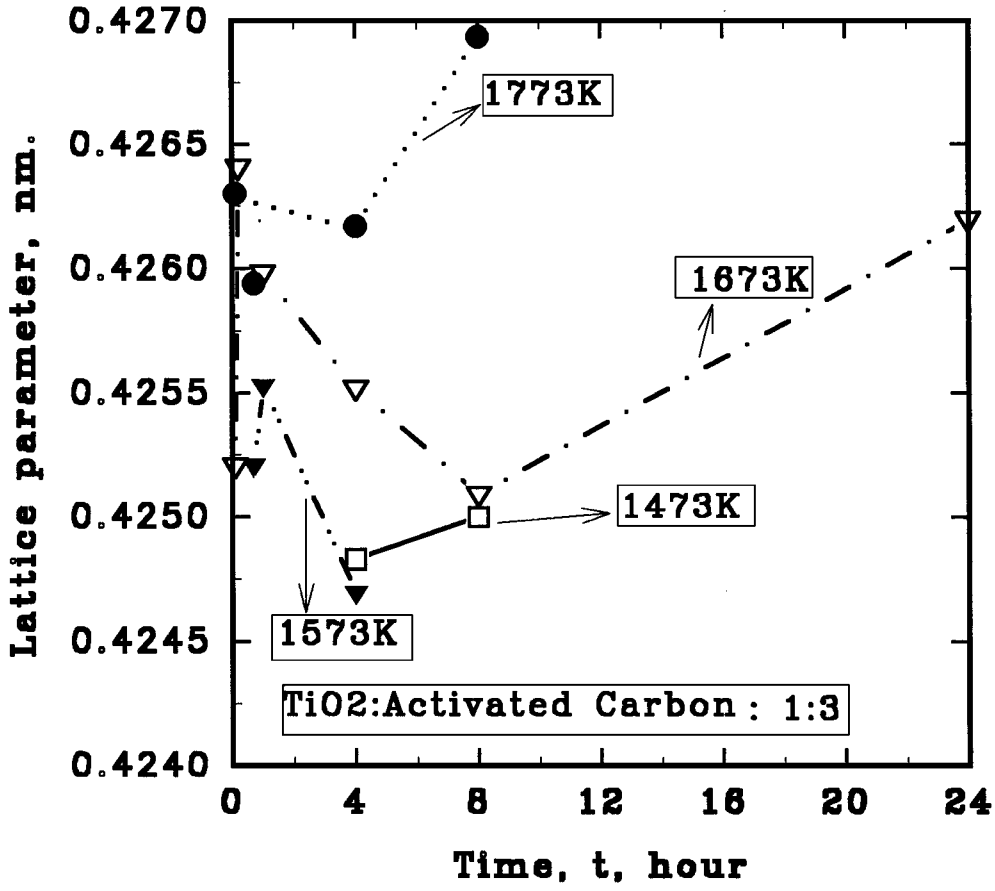

Figure 7 Effect of time and temperature on the lattice parameters of the carbonitride phase during the reduction nitridation of TiO_2 with activated charcoal (TiO_2:C = 1:3).

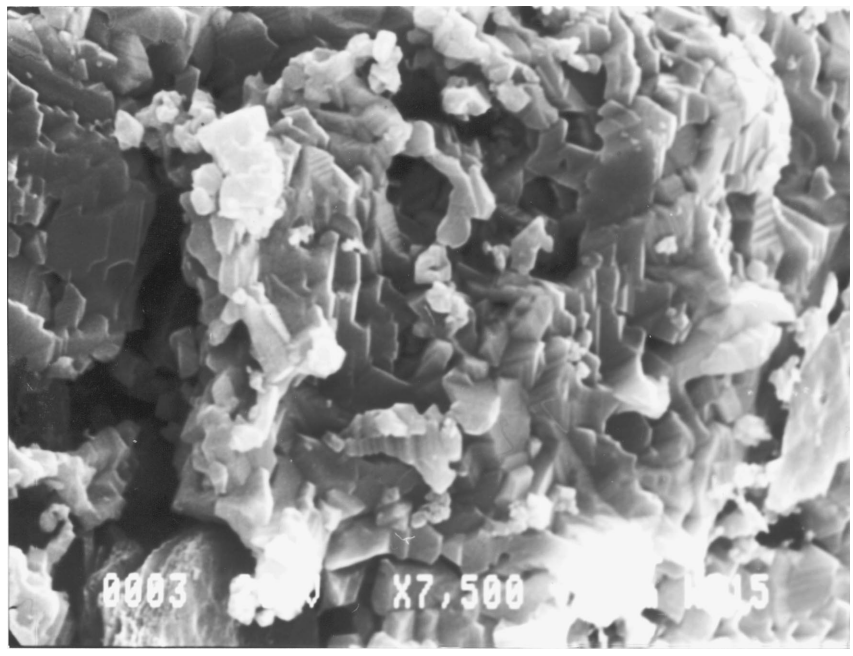

Figure 8 Microstructure of TiCN phase formed via reduction nitridation of TiO_2 with graphite in nitrogen atmosphere at 1673 K after 24 h.

5. Discussion

5.1. Phase stabilities of carbide, nitride, and oxide phases in the Ti–C–N–O system

The presence of Ti_3O_5 phase during the reduction of TiO_2 indicated that the non-stoichiometric Ti_3O_5 phase is the most stable intermediate oxide phase. In the majority of the experiments, neither TiO nor Ti_2O_3 were found to be in equilibrium with either the Ti_xN_{1-x} or the TiC_xN_{1-x} phases (see data in Table I). The reason for the absence of TiO and Ti_2O_3 can be explained on the basis of the Gibbs free energy data for the stability of suboxide phases. Using the Gibbs free energy data [27], the phase predominance area diagram in the Ti–O–C–N system is plotted and is shown in Fig. 11.

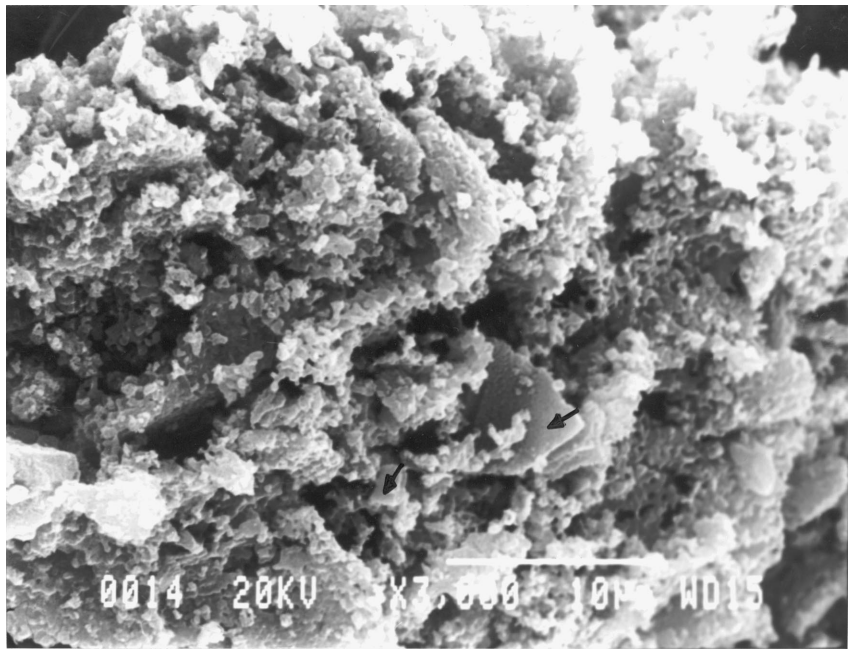

Figure 9 Microstructure of TiCN phase formed via reduction nitridation of TiO_2 with activated charcoal in N atmosphere at 1673 K after 8 h.

In Fig. 11, the stability of a phase is defined by log $P(N_2)$ and is plotted against log $P(O_2)$ at a given temperature. Here P_{O_2} and P_{N_2} are the equilibrium partial pressures of O_2 and N_2 gases, respectively, in the Ti–C–N–O system for various solid-phase combinations (Fig. 11). P_{O_2} can also be plotted as P_{CO} because the equilibrium partial pressure of oxygen (P_{O_2}) is proportional to P_{CO} via $C + 1/2\,(O_2) = CO\,(g)$ reaction (Fig. 11). The regions of stability of TiN, TiC, and suboxides are shown in Fig. 11 at 1573 K. The log (P_{N_2}) versus log (P_{O_2}) diagram (Fig. 11) and the relationships in Table VII, confirm that Ti_3O_5 phase can thermodynamically coexist with TiN phases at 1573 K, for example. In Fig. 11, the vertical lines define the iso-oxygen potentials for phases indicated and the phase boundaries between the two phases concerned. Similarly, the horizontal lines are the iso-nitrogen potentials for the carbide, carbonitride, and nitride phases and their phase boundaries. The iso-oxygen potential lines for Ti_2O_3 and TiO intersect line "ab" in Fig. 11 above 1 atm N_2 partial pressure, which means that at atmospheric pressure conditions, as adopted in the present investigations, neither of the two oxide phases are likely to be stable. Line "xy" is for $TiO + 1/2\,N_2 = TiN + 1/2\,O_2$ equilibrium at 1573 K, and this line intersects TiO, Ti_2O_3, and Ti_3O_5 at points a′, b′, and c′, which correspond to N activity of less than one. Lines "ab" and "ac" are concurrent at "a" and intersect $TiC_{0.5}N_{0.5}$ line (MN) at points p′ and p, respectively. Point p corresponds to an oxygen (O_2) potential of $p_{O_2} = 2 \times 10^{-17}$ atm, which is very close to the equilibrium value reported by Ouensanga *et al.* [28] at 1573 K for $TiC_{0.67}O_{0.33}$ phase. The vertical lines aq and p′ q′ define $TiO_xC_yN_z$ and $TiO_{0.33}C_{0.67}$ phases, respectively; the values of x, y, and z being fixed by C, N, and O activities. The fractions of interstitials x, y, and z are not known. The equilibrium relationships also show that a much lower O_2 potential than Ti_3O_5/TiN equilibrium is required for the coexistence of TiOC and Ti_2O_3 phases, as observed by Terry and Chinyamakaobvu [6]. The predominance area phase diagram is, therefore, consistent with the experimental findings in this work and by other researchers [17–19]. The reason that Terry and Chinyamakaobvu [6] observed Ti_2O_3 in equilibrium with the TiOC phase is due to the presence of Fe–Ti–C

TABLE VII Equations for the Gibbs free energy and log (P_{N_2})-log (P_{O_2}) relationships at 1573 K. Activity of carbon, $a_c = 1$. log (P_{O_2}) = x atm. Thermodynamic data have been taken from [29]

Reaction	ΔG°_T, J mol^{-1}	ΔG°_{1573} J mol^{-1}	Equations, at 1573 K log (P_{N_2}) (atm) = y
$TiO\,(s) + 1/2\,N_2\,(g) = TiN\,(s) + 1/2\,O_2\,(g)$	178 410 + 19.26 T	208 710	y = 13.85 + x
$TiO\,(s) + 1/2\,N_2\,(g) = TiON\,(s)$	−68 860 + 116.4 T	114 235	y = 7.586 + x
$Ti_2O_3\,(s) + N_2\,(g) = 2\,TiN\,(s) + 3/2O_2\,(g)$	829 830 − 71.6 T	717 200	y = 23.81 + 1.5 x
$TiC\,(s) + 1/2\,N_2\,(g) = TiN\,(s) + C\,(s)$	604 672 − 87.3 T	467 350	y = −1.638
$TiO\,(s) + C\,(s) = TiC\,(s) + 1/2\,O_2\,(g)$	329 867 − 61.5 T	233 125	x = −15.48
$Ti_3O_5\,(s) + 3/2\,N_2\,(g) = 3TiN\,(s) + 5/2\,O_2\,(g)$	1 426 158 − 140.7 T	221 320	y = 26.67 + 5/3x
$Ti_3O_5\,(s) + 3C\,(s) = 3TiC\,(s) + 5/2\,O_2\,(g)$	1 880 792 − 382.8 T	278 645	x = −13.98
$Ti_2O_3\,(s) + 2C\,(s) = 2TiC\,(s) + 3/2\,O_2\,(g)$	1 132 525 − 233 T	766 016	x = −14.96
$Ti_{0.67}O_{0.33}\,(s) = 0.67TiC\,(s) + 0.33\,TiO\,(s)$	—	253 580	x = −16.77

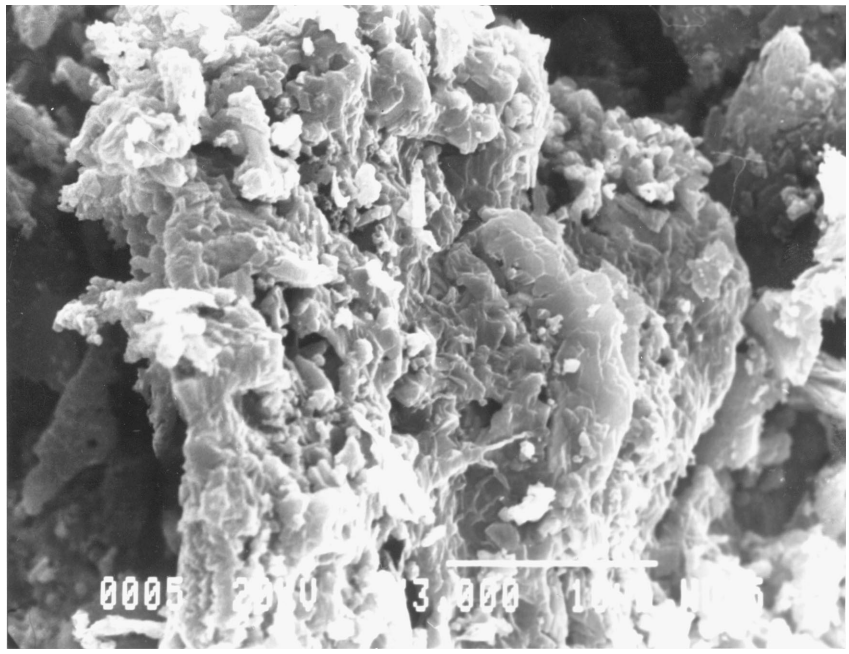

(a)

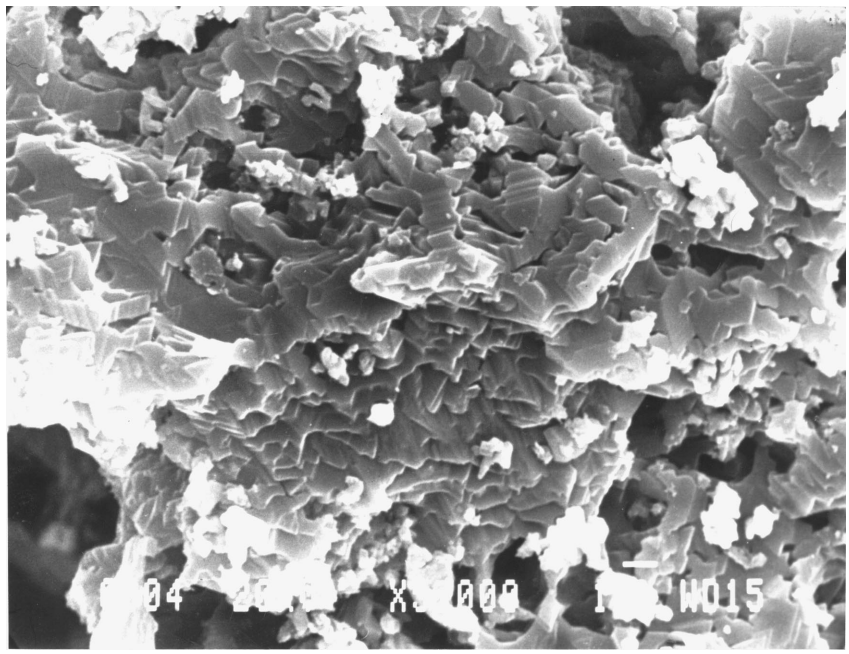

(b)

Figure 10 Microstructure of the reaction product at different time intervals with graphite and activated charcoal. T = 1673 K. (a) sintered Ti_nO_{2n-1} with TiCN on surface after 1 h of reduction with graphite, (b) growth of faceted TiCN phase after 8 h of reaction, (c) fine TiCN particles formed with activated charcoal after 1 h, (d) sintering of TiCN phase after 8 h of reaction with activated charcoal. TiCN produced from activated charcoal reduction does not sinter rapidly compared with faceted TiCN formed from graphite.

alloy during the reduction of ilmenite ($FeTiO_3$) with C. The thermodynamic activities of TiC and TiO are also lowered in equilibrium with metallic iron.

5.2. The mechanism of nitridation of TiO_2 in the presence of C

The rates of reduction curves shown in Figs 3 and 4 agree with the lattice parameter changes in Figs 6 and 7 for simultaneous reduction-nitridation of TiO_2 with graphite and activated charcoal, respectively. It is also evident from the X-ray diffraction analysis of phases formed that Ti_3O_5 and TiCN phases coexist over a range of temperatures and time. This evidence is consistent with the observations made by previous researchers [15–20].

In Figs 6 and 7, the change in the cell dimension of TiCN phase is shown as a function of time, and we find that in the very first stage with activated charcoal, for example, the TiCN phase formed is much richer in C than in N. As a result, the TiCN formed rapidly approaches towards the TiC equilibrium composition by lowering the N_2 and O_2 partial pressures (i.e., line ap′b in Fig. 11) via $TiN + xC = TiC_xN_{1-x} + x/2\ N_2$ reaction. The lowering of N_2 partial pressure in the early stage of reaction as a result of the formation of C-rich TiCN at a given temperature enables oxides such as Ti_3O_5 to react and

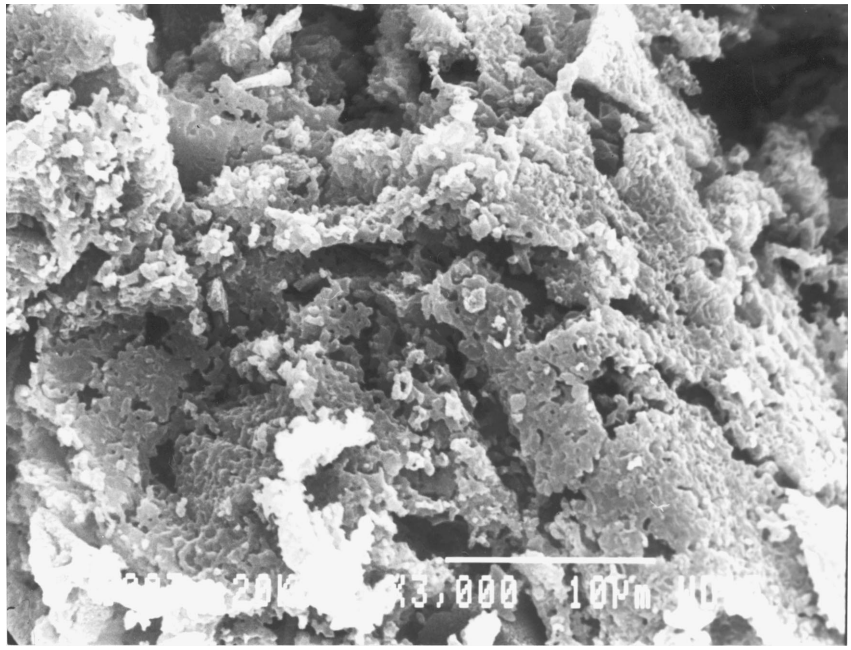

(c)

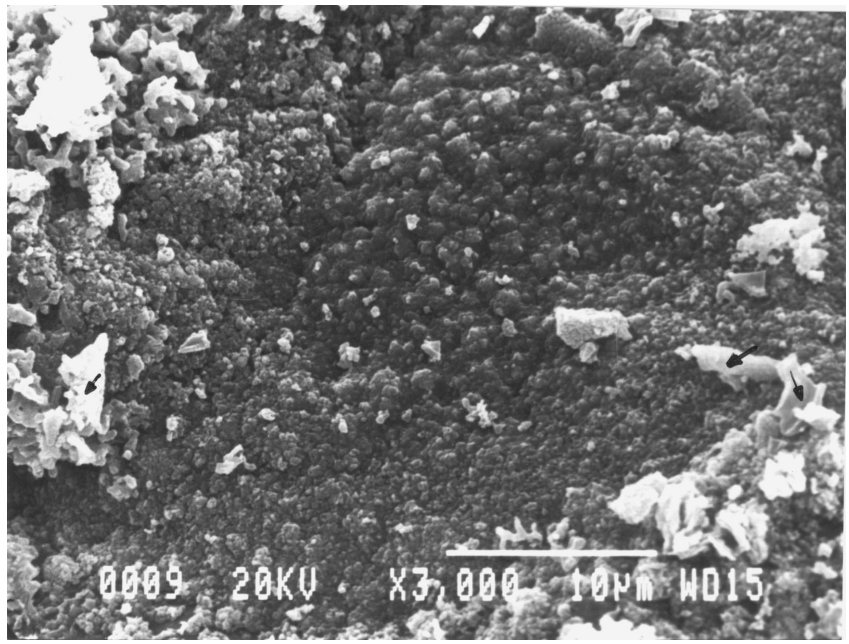

(d)

Figure 10 (*Continued*).

produce an O-containing TiCN phase, as observed by Licko and co-workers [18] via reaction between C-rich TiCN and Ti_3O_5. The replacement of C by O at the interstitial sites in the TiCN structure results in a decrease in the lattice parameter (see Figs 6 and 7), as seen in the second stage (regime II) of the overall reaction. As the overall O content of the mixture drops, the C dissolution in the TiCN lattice recommences, which is indicated by the increase in the lattice parameter of the TiCN phase in the final stage (regime III). The slow rate of loss of O from the TiOCN phase is consistent with the smallest slope for the percentage reduction versus time curves in Figs 3 and 4 in regime III. The rate of change of lattice parameter as a function of time is strongly dependent on the temperature and is also related to the equilibrium solubilities of C, O, and N in the TiCN lattice. The presence of the vacant interstitial sites in the TiCN phase is responsible for the dissolution of C, O, and N. Because of the stability of mixed interstitial phases with the suboxides of Ti, the interstitial concentration in B1-NaCl structure changes gradually via a diffusion process. In conclusion, the diffusion of interstitial atoms in TiCN phase plays the most important role in determining the overall rate of reaction.

5.3. Interpretation of the activation energy data

The plot of the rate of reaction (d%R/dt) for activated carbon and graphite is shown in Fig. 12 and are compared with the calculated O diffusivity in TiO_2 (also in B1-NaCl lattice), which can be obtained from

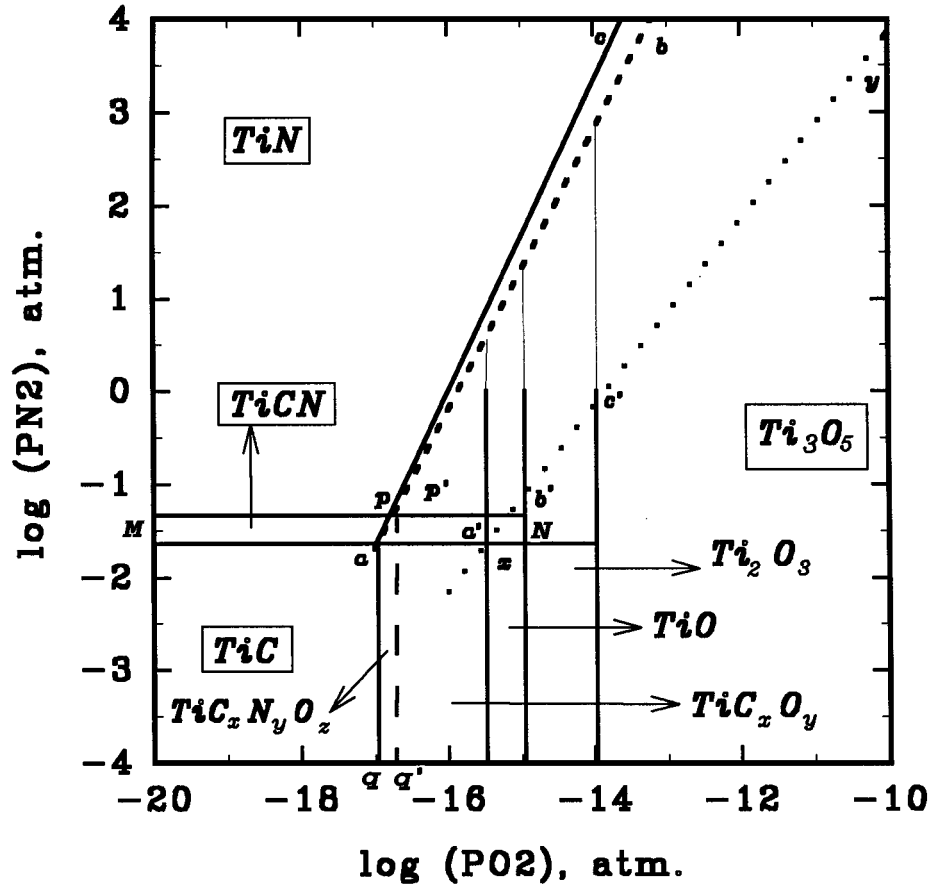

Figure 11 Calculated predominance area diagram for stable phases at 1573 K in the TiCN system. Activity of carbon, $a_c = 1$.

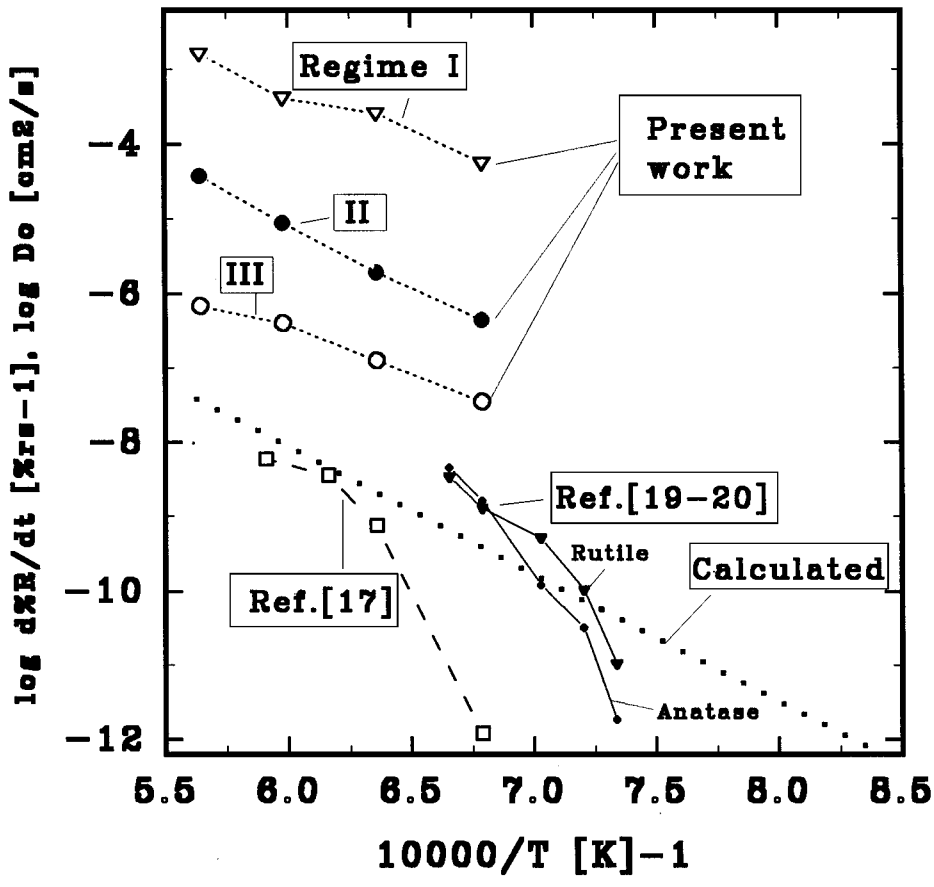

Figure 12 A comparison of the measured rates of overall reaction in three regimes of $TiO_2 \rightarrow$ TiCN formation process with the calculated diffusion rates for interstitial species in the B1–NaCl structure.

Equation 3 [29].

$$D_O = (\gamma \cdot \upsilon \cdot \alpha^2) \cdot \left(1/4 \cdot \left(P_{O_2}\right)^{1/2}\right)^{0.33} \cdot \exp\left(-\frac{\Delta G_O}{3\kappa T}\right) \cdot \exp\left(-\frac{\Delta G^*}{\kappa T}\right) \quad (3)$$

In this equation, D_O is the O diffusion coefficient ($cm^2\,s^{-1}$), γ is called the geometric factor and has a value of 0.1, υ is the frequency factor ($10^{13}\,s^{-1}$), α_O is the jump distance (3.248×10^{-8} cm), ΔG_O is the free energy of solution assuming that the vacancies behave as a solute, ΔG^* is the activation energy for O diffusion in TiO_2 lattice is (190 kJ mol^{-1}) [29], and P_{O_2} is the equilibrium O partial pressure (atm). κ is the Boltzmann constant. This equation is based on the diffusivity of O through vacant sites in the TiO_2 lattice.

The slope of the line for calculated D_O values plotted against 1/T in Fig. 12 is similar to the observed slopes for the rates of nitridation and reduction with activated charcoal and graphite. The comparison of the temperature coefficient of the rate processes indicate that the O-deficient sites in TiO or even in the TiO_2 lattice (for which the eq.4 is also valid; see [29]) is the rate-determining step. The computed values of activation energy 230 kJ mol^{-1} compare well with the experimental data for the activation energy (220–240 kJ mol^{-1}) with graphite for the three regimes of reaction indicated previously (the slope is $-Q/2\kappa$). These values also agree with the value of 260 kJ mol^{-1} reported by Li and Riley [17] in the temperature range 1473 to 1693 K. The difference of 30 kJ mol^{-1} for the high temperature rate data above 1473 K between the work of Li and Riley and the present work may be due to the small difference in the temperature range and the concentration of gas used by Li and Riley, which was N_2 plus H_2 compared with pure N_2 in this study. The presence of H_2 in the gas phase makes the reduction process thermodynamically less favourable, and it may therefore reduce the concentration of vacancies needed for interstitial diffusion. The value of apparent activation energy in the present investigation is, however, significantly smaller than those published by White *et al.* [19, 20] in the temperature range 1163 to 1503 K. The observed difference in the values of activation energies determined by White *et al.* [19, 20] and in this work could be due to the temperature range over which the reduction nitridation reaction was studied. The diffusion mechanism in O-deficient oxides changes as a function of temperature and pressure [29]. At lower temperatures, the values of activation energies are higher because the O ion migration is influenced by the presence of impurities and the solubility of O, which is lower at lower temperatures.

6. Conclusions

1. The simultaneous reduction and nitridation of TiO_2 to TiCN phase in the presence of C, $CO + C$, and $CO + H_2 + C$ as reducing agents in a N atmosphere progresses by forming suboxides (Ti_nO_{2n-1}), where n varies between 3 and 5. The value of n depends on time. At an early stage of the reduction-nitridation, higher n suboxides of titanium form, whereas at a later stage, only Ti_3O_5 forms in equilibrium with TiCN phase. We have not found any evidence for the presence of either TiO and Ti_2O_3. The observation for the presence of oxide phases is consistent with the phase predominance area diagram in the Ti–C–N–O system.

2. Activated charcoal was found to be a more effective reducing agent than graphitic C. As a result, the overall rate of reduction nitridation was found to be much faster in the case of charcoal than with graphite.

3. The apparent activation energy (230 kJ mol^{-1}) in the temperature range 1473 to 1773 K for the reduction nitridation appears to correspond to the diffusion of O or interstitial atoms in the cubic B1 structure of TiO or TiCN. The value of the activation energy was found to be comparable with the 260 kJ mol^{-1} data derived by Li and Riley [17] for the temperature range 1473 to 1693 K.

4. The lattice parameter of B1 phase was found be strongly dependent on the reducing atmosphere conditions. The lattice parameters of TiCN phase with various C:N ratios, however, appear to lie closely to the straight line joining the vales of stoichiometric TiC and TiN, indicating that TiC and TiN form a continuous solid solution. The solid solubility also appears to extend into the TiO phase field.

References

1. H. J. GOLDSCMIDT, "Interstitial alloys" (Butterworths, London, New York, 1967).
2. L. E. TOTH, "Transition metal carbides and nitrides" (Academic Press, New York, 1971) pp. 71–89.
3. B. NORTH, KennaMetal Inc. Pittsburgh, PA, private communication.
4. S. K. RHEE, *J. Amer. Ceram. Soc.* **53**, (1970) 388.
5. J. KELLIE and J. V. WOOD, *Materials World* **Jan** (1995) 10–12.
6. B. S. TERRY and O. CHINYAMAKAOBVU, *Materials Science and Technology* **7** (1991) 842–848.
7. A. K. LEE, L. E. SANCHEZ-CALDERA, S. T. OKTAY and N. P. SUH, *Advanced Materials & Processes* **8** (1992) 31–34.
8. P. GRIEVESON, *Proc. Briti. Ceram. Soc.* **8** (1967) 137–153.
9. B. CALES, in "Ceramic matrix composites," 2nd European Symposium on Engineering Ceramics, edited by F. L. Riley (Elsevier Applied Science, 1989) p. 198.
10. T. AKASHI, A. SAWAOKA and S. SAITO, *J. Amer. Ceram. Soc.* **61** (1978) 245–246.
11. P. DUWEZ and F. ODELL, *J. Electrochem. Soc.* **97** (1950) 299.
12. M. EL-GRAMI and Z. A. MUNIR, *J. Amer. Ceram. Soc.* **73** (1990) 2222–2227.
13. *Idem, ibid* **73** (1990) 1235–1239.
14. A. DOI, N. FUSIMORI and T. YOSHIOKA, *Inst. Phys. Conf. Ser.* **75** (1986) 743.
15. V. D. LYUBIMOV, *Neorg. Mater.* **13** (1977) 58–62.
16. S. UMEZU, *Proc. Imperial Academy (Tokyo)* **7** (1931) 353–356.
17. WEN-YU LI and F. L. RILEY, *J. Eur. Ceram. Soc.* **8** (1991) 345–354.
18. T. LICKO, V. FIGUS and J. PUCHYOVA, *ibid* **5** (1989) 257–265.
19. G. V. WHITE et al. *J. Mater. Sci.* **27** (1992) 4294–4299.
20. *Idem, ibid* **27** (1992) 4300–4304.
21. C. BODSWORTH and H. B. BELL, "Physical chemistry of iron and steel manufacture," 2nd ed. (Longman, London, 1972) pp. 124–127.
22. *Idem, ibid* (Longman, London, 1972) pp. 312–315.

23. C. H. P. LUPIS, "Chemical thermodynamics of materials" (Elsevier Science Publ., New York, 1983) pp. 518–521.
24. S. ANDERSSON, B. COLLEN, U. KUYLENSTIERNA and A. MAGNELI, *Acta. Chem. Scan.* **11** (1957) 1641–1652.
25. P. L. WALKER, M. SHELEF and R. A. ANDERSON, in "Chemistry and physics of carbon," Vol. 4, edited by P. L. Walker (Edward Arnold Ltd., London, 1968) pp. 287–301.
26. E. T. TURKDOGAN and J. V. VINTERS, *Carbon* **8** (1970) 39.
27. E. T. TURKDOGAN, "Physical chemistry of high-temperature technology" (Academic Press, New York, 1980) pp. 4–25.
28. A. OUENSANGA, *J. Less Common Metals* **79** (1981) 237–241.
29. W. D. KINGERY, H. K. BOWEN and D. R. UHLMANN, "Introduction to ceramics" (John Wiley, New York, 1976) pp. 239–247.

Received 16 March
and accepted 28 July 1998